Article:

Forlati, G. and Shepley, P. (2021) Tensile response and fracturing process in moderate and high plasticity clays. Canadian Geotechnical Journal, 58 (3). pp. 317-327. ISSN 0008-3674

https://doi.org/10.1139/cgj-2019-0082

Canadian Science Publishing | Canadian Geotechnical Journal

Tensile response and fracturing process in moderate and high plasticity clays

Journal:	*Canadian Geotechnical Journal*
Manuscript ID	cgj-2019-0082.R3
Manuscript Type:	Article
Date Submitted by the Author:	17-Apr-2020
Complete List of Authors:	Forlati, Giulia; University of Sheffield, Department of Civil and Structural Engineering Shepley, Paul; University of Sheffield, Department of Civil and Structural Engineering
Keyword:	clay, fracture, tension, moisture content, sinkhole
Is the invited manuscript for consideration in a Special Issue? :	Not applicable (regular submission)

TENSILE RESPONSE AND FRACTURING PROCESS IN MODERATE AND HIGH PLASTICITY CLAYS

Forlati Giulia, PhD, Department of Civil and Structural Engineering, University of Sheffield, South Yorkshire, UK

gforlati1@sheffield.ac.uk[1]

Dr Paul Shepley, Lecturer in Geotechnical Engineering, Department of Civil and Structural Engineering, University of Sheffield, South Yorkshire, UK

p.shepley@sheffield.ac.uk

For correspondence:

Giulia Forlati

Via Fallmerayer 1

39042, Bressanone (BZ)

Italy

giulia.forlati@gmail.com

+39 348 8767572

---

[1]Current affiliation and address:
Giulia Forlati, Researcher, Dipartimento di Ingegneria Ambientale e Meccanica (DICAM), Universitá di Trento, Italy. giulia.forlati@gmail.com

ABSTRACT

Sinkholes in clay soils can be considered as the collapse of a soil layer previously bridging a void. Here, flexural deformation in the clay drives the formation of tensile cracks from the lowest surface of the layer and the consequent soil collapse is from crack propagation. Considering a simplified model of the sinkhole geometry, this paper aims to describe the tensile and fracture behaviour of clay soils with different plasticity indices. Speswhite kaolin, London and Durham clays were tested using direct tensile and bending tests. Moderate and high plasticity clays showed a nonlinear fracture response with increasing moisture content, while low plasticity clays demonstrated a linear response. Bending tests confirmed the importance of the moisture content while the plasticity index confirmed the difference in ductile or fragile collapse for fracture propagation. To assess the results, Elasto-Plastic Fracture Mechanics (EPFM) theory was applied to clays with appropriate modifications. The analysis demonstrated that EPFM theory provides a good baseline for predicting tensile fracture behaviour in clay soils which can be extended in future research.

Key words

Clay, tensile, fracture, moisture content, strength, sinkholes

1. INTRODUCTION

Sinkholes are caused by the collapse of the ground into underlying cavities created by karst terrain or former mine workings and are a common hazard in many countries (Waltham et al. 2005). The UK is particularly affected by sinkholes, which have increased in the last 20 years due to increasingly severe wet and dry periods (British Geological Survey 2013). Commonly the surface material is cohesive in nature, hence its ability to bridge the cavity below, but this can lead to sudden catastrophic collapses. Therefore, predictive methods are urgently needed to assess the likelihood of sinkholes.

Geotechnical investigations are not usually carried out after the events, as sinkholes are believed to be not important anymore. However, the geotechnical characterisation of the soil overlying the rock cavity is important to understand how a sinkhole forms. Limited research has been conducted on sinkhole formation, in most of the cases with a focus on sandy material behaviour (Abdulla and Goodings 1996; Bronkhorst and Jacobsz 2014). It is clear that more work is required on clayey materials due to their ability to be temporarily stable before collapse. It is reasonable to hypothesise that tensile cracks can develop along the basal edge of the layer of the soil cover that is bending, as tensile forces determine stresses that exceed the tensile strength of the clay. Therefore, the propensity for crack formation influences the collapse point and the formation of a sinkhole. The work described in this paper aimed to study the behaviour of clays with different plasticity index in tensile and bending conditions in order to demonstrate the relationship between the fracture mechanism and the variation of moisture content. The study presented might be considered as a starting point for the research on the behaviour of clay soils overlying underground cavities.

The fracture mechanics theory, already established in metallurgy, is used to understand how tensile fractures form and lead to sinkholes. Specifically, the elasto-plastic fracture mechanics (EPFM) approach has been adapted from metals to be applicable to clays. Fracture mechanics approaches the formation of cracks based on specific material properties in the process zone immediate to the crack notch, rather than solely on the bulk tensile resistance of the material. Given the difficulty of predicting the bulk tensile resistance of clays, using fracture mechanics may provide a novel approach for assessing failure mechanisms in fine grained soils.

2. PREVIOUS WORK

The term sinkhole is used to identify a site where the ground is sinking into a void (Waltham et al., 2005; Donnelly, 2008). The term spans different processes of formation which are represented by different types of sinkholes (solution, collapse, dropout, buried, caprock and suffusion sinkholes). However, only one type of sinkhole forms rapidly in clayey soils producing the most catastrophic effects and it is named “dropout sinkhole”. The dropout type of sinkhole takes place where an underground void (caused by water dissolution of soluble rock or former mine workings for example) is overlain by a layer of cohesive soil and the presence of a void leads to sagging bending in the overlying clay. It has been hypothesised that such flexural deformation of the clay layer causes cracks to form in the basal chord of the clay and the consequent dropout of part of the zone into the cavity below, leaving the remaining clay layer in an arch configuration. With further water percolation, the arch increases in size, bending to its maximum loading capacity and then fails due to the propagation of fractures. This leads to the outright collapse of the clay layer creating a void at the surface (Figure 1). Sinkhole cavities are usually spherical or funnel-shaped and form a circle hole at the ground level. For this study, a sinkhole was hypothesised to form in a continuous clay layer simplified as a beam spanning the entire cavity, with fully-fixed ends to represent the continuous nature of the clay layer (Figure 2). The model adopted allowed to simplify the clay layer in the simplest manner omitting the study of the arch formation and progressive failure of in the clay layer. The study is applicable to sinkholes formed in shallow clay layers.

In order to span the void, the clay deforms developing tensile stresses in the central section that drive crack formation which is hypothesised to have a key role in the sinkhole formation. Tensile cracks emanate from the bottom edge where the ultimate tensile strength is exceeded while mixed mode cracks appear at the fixed beam extremities due to the presence of moment and shear. In this study, a simpler mechanical model than the fully-fixed ended beam is adopted. The clay layer is simplified as a simply supported beam in which only tensile cracks appear due to the importance of the central section in the hypothesised sinkhole collapse mechanism.

Cracking behaviour is controlled by the mechanical parameter tensile strength which in metallurgy is governed by the metal's crystalline structure. In clays it is reasonable to suggest that tensile strength is predominantly influenced by moisture content, plasticity index and compaction. Ajaz & Parry (1975) and Stirling et al. (2015) showed that the main difference in tensile behaviour is caused by variations in moisture content. An increase of moisture content determined a decrease of tensile strength and an increase of the tensile strain. Later, Tang et al. (2015) showed that compaction density has an important role in the determination of tensile strength, which increases with increasing dry densities.

Where tensile strength and fracture processes have been previously studied, a range of approaches have been used due to the lack of a standard method.

Wang et al. (2007a) and Amarasiri et al. (2011) studied the tensile behaviour of clays, applying the concepts of the linear elastic fracture mechanics (LEFM). Experiments showed a linear-elastic behaviour, with tensile strength and fracture toughness reducing with increasing moisture content. The soils cracked in a brittle manner even if they were in a wet condition with a moisture content higher that the optimum moisture content. However, the results from Amarasiri et al. (2011) showed samples still failed in a brittle manner but the measured fracture toughness had a high value, suggesting ductile fractures. They also found that a dry clay deformed more than a wet clay. Overall, their results demonstrated that clay samples did not behave in a linear elastic manner and therefore the application of a linear elastic analysis was unrealistic, especially for wet clays.

Hallett and Newson (2001, 2005) instead used the elasto-plastic fracture mechanics (EPFM) to study the fracture behaviour of mixtures of kaolinite and silica sand. The use of the EPFM was justified by the nonlinear response of the beams in bending. Hallett and Newson (2001, 2005) used the parameter crack tip opening angle (CTOA) to characterise the initial notch opening in deforming soft soils. They showed that the CTOA decreased with the reduction of the plasticity index, which was controlled by adding sand with the clay mixture. But the CTOA was not used in other research on clay behaviour, questioning the utility of CTOA as being a unified approach to characterise the mechanism of crack propagation.

Due to the uncertainties on a reliable method to apply for studying fractures in clay, we can look towards the Elastic-Plastic Fracture Mechanics (EPFM) widely applied to metals. Standard testing procedures and methods to determine the fracture toughness can be found in the ASTM E1820-15 (2015), where standard geometry and formulas are used to determine the fracture toughness J_{IC} and the crack tip opening displacement CTOD. These two properties may be able to represent a clay's fracture behaviour in a more unifying manner than seen previously.

3. METHOD

MATERIALS

Three different clays of different plasticity index (PI) were used in the tests: Speswhite kaolin, London clay and Durham clay. All clays were reconstituted before testing. Figure 3 reports typical particle size distributions found by Murillo et al. (2013), Toll et al. (2012) and Gasparre (2005). The clay properties are listed in Table 1. The Atterberg limits for kaolin, Durham and

London clays were calculated as part of the investigation. The activity of the clays was calculated using the clay fraction of the typical particle size distributions shown in Figure 3. Kaolin and Durham clays had an activity lower than 0.75, which classified both the clays as inactive. London clay had an activity ranging from 0.58 to 0.99 and it was classified respectively inactive or normal clay. The optimum moisture content ω_{OMC} was calculated for kaolin clay through the compaction test (BS 1377:1990 Part 4). The ω_{OMC} of Durham and London clays was determined from the literature (Glendinning et al., 2014; Sivakumar et al., 2015; Mavroulidou et al., 2013). The Durham clay was composed of various amounts of illite/smectite, chlorite/smectite, illite and kaolinite (Glendinning et al., 2014). The main minerals that composed the London clay were poorly crystalline kaolinite, illite, chlorite, smectite and montmorillonite (Gasparre, 2005).

SAMPLE PREPARATION

All three clays were obtained by the consolidation of clay slurry mixed to 1.2 times the liquid limit, ratio lower than the typical 2 times the liquid limit. The low ratio adopted was based on the need to obtain samples' heights higher than 100 mm at the end of the consolidation process. A double height (*h*=250 mm), 250 mm diameter Rowe cell was used to bring the vertical pressure to 200 kPa in incremental loading stages. 110-130 mm-high clay samples were obtained at the end of the consolidation process. Small beam samples were cut from the consolidated clay blocks and then oven dried to obtain a range of different moisture contents. The samples were dried for 0, 30, 90, 150 minutes in a 40 ºC oven. A thorough analysis of the moisture content distribution within a test beam sample for each drying condition demonstrated a constant moisture content at all points in the cross section and along the beam length. An average of 10 samples for each clay was used in the direct tensile tests, with 2 samples for every moisture content. An average of 30 samples for kaolin and Durham clays were studied in bending, with 2 samples per moisture content. Fewer samples were performed using London clay due to the small volume of material available.

SETUP

The tensile behaviour was tested using direct tensile and beam bending experiments. The methodology was adapted from standard metal testing to demonstrate its applicability on soils. For the direct tensile experiments, an AGS-X Shimadzu loading frame with a mobile brace moving upwards was used (see Fig. 4a). According to the ASTM E8/E8M-15a (2015) standard about tensile tests on metallic materials and the tensile tests performed by Tschebotarioff et al. (1953) and Lakshmikantha et al. (2008), samples were cut from the clay blocks using a wire cutter and a preformed template. Samples were shaped as a dog bone, measuring 70 mm (L) in length (Fig. 5a). The extremities of the samples had a squared cross-section and dimensions of 25x20 mm (BxW), while the central part where the crack formed measured 5x20 mm in cross-section (B_0xW). The samples were glued to the top and bottom supports using epoxy resin. To avoid the detachment of the sample from the supports, the epoxy resin covered both the large extremities of the samples. A smaller central area with a constant section causes tensile cracks to form in this region where the stress was constant. Samples were pulled apart at a strain rate of 1 mm/min until rupture.

Bending tests were performed using the same equipment but with the mobile brace moving downwards (see Fig. 4b). Square-section beams of dimensions equal to 20x20x100 mm (BxWxL) were positioned on the base supports using two rollers placed at a distance of 80 mm (S_P) from each other (see Fig 5b). An initial notch of 10 mm (a_0) was cut using a wire cutter in the bottom edge of the middle section of the beam to facilitate the formation of mode I (tensile) cracks. The geometry was chosen based on the geometry adopted in previous bending tests (Amarasiri et al. 2011; Hallett and Newson 2001, 2005) which was taken from the typical geometry used in metal bending tests. The geometry suggested in ASTM E1820-15 (2015) uses the ratios *L=4-5W*, *W=2B* and *a=1/2-1/3W*, where *L* is the beam length, *W* the beam height, *B* the beam width and *a* the length of the initial notch. The difference between metal and soil beams consisted in the measure of the beam's width *B*, which in soil was chosen to be equal to the beam's height *B=W* and not as *B=0.5W* to prevent the clay deforming on the roller supports. Hallett and Newson (2001, 2005) placed two rigid supports under the two specimen's halves. The beam was sustained by two glass slides that were free to move on the rollers. Beams supports were not used in this investigation because they were considered elements of resistance to the load application. Without them, specimens were affected by the gravity force. However, the setup was considered more similar to a real in-situ problem. A point load was then indirectly applied at the top of the middle section of the beam imposing a constant strain rate of 1 mm/min. The same strain rate was used for direct tensile and bending tests.

4. RESULTS

The load and displacement experiment data were converted into stress and strain. For the direct tensile tests, the conversion from load-displacement to stress-strain graphs was obtained dividing the applied load *P* by the initial cross-sectional area A_0 of the sample:

$$\sigma_t = \frac{P}{A_0} \qquad (1)$$

The use of the initial cross-sectional area assumed there was no significant necking effect during loading, as was observed during testing. Because the epoxy resin covered both the large extremities, those were considered as part of the rigid supports. Therefore, the strain was calculated as the ratio of the length increment over the original length of the section with a constant area

$$\varepsilon = \frac{\Delta \mathrm{L}}{\mathrm{l}_0} \qquad (2)$$

where ΔL is the length increment and l_0 is the original length of the sample section with a constant area.

Despite the nonlinear behaviour shown during bending tests, the load was converted into global stress considering linear elastic conditions. De Saint Venant formulas were used on the net section of the bending beams in order to calculate a first approximation of the tensile stress at the crack tip (Figure 6):

$$\sigma_t = \frac{M}{I} y \tag{3}$$

$$I = \frac{1}{12} B (W - a_0)^3 \tag{4}$$

$$y = \frac{W - a_0}{2} \tag{5}$$

$$M = \frac{P S_p}{4} \tag{6}$$

in which σ_t is the tensile stress developed at the bottom edge of the beam, M is the moment generated from the beam bending, I is the moment of inertia of the cross-sectional area of the beam, B is the beam width, W is the beam height, a_0 is the initial crack length, P is the load sustained by the beam and S_p the beam span. The use of De Saint Venant allowed to ignore the effects caused by the application of a point load on soft clays.

Tensile strain was calculated with the formula proposed by Viswanadham et al. (2010). A first approximation of the tensile strain at the bottom edge of the clay beam was determined using a linear elastic relationship as:

$$\varepsilon = R_{0f} k W \tag{7}$$

Where R_{0f} is the neutral layer coefficient, defined as the ratio of the vertical distance of the neutral layer from the top surface of the beam to the depth of the soil beam, $k=1/R$ is the curvature of the beam along the centreline. R is the radius of maximum curvature, computed as follows:

$$R = \left(\frac{\Delta}{2} + \frac{L^2}{8\Delta}\right) \tag{8}$$

where Δ is the vertical displacement and L is half of the length of the sample.

Due to the geometry adopted for testing kaolin, London and Durham clays, $L=S_p/2$. The equation to calculate the radius of curvature was modified as:

$$R = \left(\frac{\Delta}{2} + \frac{S_p^2}{32\Delta}\right) \quad (9)$$

Typical results in terms of stress and strain obtained from the direct tensile and bending tests are reported respectively in Figure 7 and 8. In the direct tensile tests, samples developed an increasing force with increasing displacement. Once the maximum force was reached, the samples broke in the middle section due to the formation and propagation of tensile cracks. The ultimate tensile strength was defined as the maximum value of stress sustained in a sample before breaking. In bending tests, attainment of the maximum force did not always correspond to crack formation. The different point of crack initiation is visible in Figure 8, in which the stress-strain graphs of three kaolin samples having moisture content equal to ω=44.8%, 42.1% and 38.8% ($\omega/LL = 0.69,\ 0.65,\ 0.60$) are plotted. For samples with a high moisture content the crack propagation was visible only after the peak stress. The kaolin sample with a moisture content of 44.8% showed a visible crack after the peak stress. In samples with a lower moisture content, for example a moisture content of 42.1%, the moment at which the crack formed and propagated corresponded to the point of maximum stress. For samples with the lowest moisture content, the crack formed before the peak stress was reached. Tensile and bending strengths are reported in Figures 9 and 10 in relation to the normalised moisture content. The normalised moisture content was obtained dividing the moisture content of the tested samples by the liquid limit (Table 1). Figures 11 and 12 show the relationship between the strain measured at the maximum stress (tensile and flexural strength) and moisture content. Moisture content was normalised against the liquid limit to highlight the change in behaviour of wet clays.

5. DISCUSSION

STRESS-STRAIN BEHAVIOUR

The clay behaviour in tensile conditions was markedly nonlinear, except in the case of Durham clay (Figures 7 and 8). Initially, kaolin and London clay beams deformed following a direct proportional line between stress and strain, suggesting a linear elastic field. Once the yielding stress was reached, the relationship between tensile stress and strain became nonlinear and the clays showed a strain hardening behaviour. This strain hardening continued until the maximum stress was reached. The maximum stress was defined as tensile strength in the direct tensile tests and flexural strength in the bending tests. At this point a tensile crack appeared in the middle section of the samples and it grew with continued deformation. With the proceeding crack growth, samples were unable to sustain the applied load and they collapsed through crack propagation. Durham clay beams followed a nearly linear elastic relationship from the beginning of the test. Samples failed in an almost instantaneous manner after reaching the flexural strength. This response was expected as the Durham clay contains fine and coarse grained particles and had a much lower plasticity index.

Moisture content played an important role in the fracturing process. This is linked to the approach used to prepare the samples because the drying process had the effect to increase the clay suction and consequently increase their strength. However, the decrease in degree of saturation and suction was not measured during the tests. In the moisture content range studied ($0.25 \leq \omega/LL \leq 1.00$), decreasing values of tensile strength were measured with increasing moisture content. A steep nonlinear reduction in strength was recorded for normalised moisture contents in the range 0.25-0.60 (Figure 9). Few samples with a normalised moisture content lower than 0.25 were tested and did not allow the definition of a specific trend. For this reason, a general behaviour and fitting line were not developed for the entire range of moisture content studied ($0.10 \leq \omega/LL \leq 1.00$).

The maximum values of strength were recorded for moisture contents equal to $0.36LL = 23.40\%$ for kaolin, $0.33LL = 13.76\%$ for Durham clay and $0.30LL = 22.59\%$ for the London clay. The small number of samples with a normalised moisture content lower than 0.25 gave a tensile strength lower than that calculated from samples with moisture content around 0.3-0.4 times the liquid limit. Thus, the maximum tensile strength was taken as the maximum value recorded for the set of samples. High values of tensile strength were recorded for London clay samples (>600 kPa) while low tensile strength values were recorded for Durham clay samples (190 kPa). Kaolin showed a maximum tensile strength (350 kPa) in between the values found for London and Durham clays. The data found by Ajaz & Parry (1975), Lakshmikantha et al. (2008), Tang et al. (2015), Stirling et al. (2015) were used to compare the tensile behaviour (Figure 13). In the figure, the moisture contents found in literature were normalised with the optimum moisture content, as the compaction method was used to prepare the samples. The moisture contents of the samples studied in this work were normalised with the liquid limit because they were obtained by consolidation. Looking at the literature data, the clays showed a similar behaviour when the moisture content ratio ω/ω_{OMC} was higher than 1.2, where the samples were considered wet. The similar response was visible in the results found by Ajaz & Parry (1975), Tang et al. (2015) and Stirling et al. (2015), while the values of tensile strengths found by Lakshmikantha et al. (2008) were lower than the other strength data. The normalised moisture contents used to study kaolin, London and Durham clays were smaller compared to those found in literature, but the tensile strengths of kaolin, London and Durham clays showed higher values than those found in literature. Only Stirling et al. (2015) tensile strength magnitudes can be compared with the tensile strength obtained in the direct tensile tests on kaolin, London and Durham clays.

Figure 10 shows the results from the bending tests. Like the tensile strength, the flexural strength shows a decreasing trend when the moisture content is increased. The results showed some scatter related to the drying process that kaolin, Durham and London clays were affected during the tests. The gravity force and a possible initial deflection of the central area of the samples could have influenced the results. Both the tensile and flexural strengths are plotted in Figure 14 in relation to the normalised moisture content. The graph shows that the strength of the studied clays was affected by the type of tensile test performed and by the plasticity index of the clay. For both the tests a high or moderate plasticity index corresponded to a high tensile or flexural strength, as it is shown for London and kaolin clay samples. A low plasticity index determined a low tensile or flexural strength as seen in the Figure 14 for Durham clay samples. However, the nonlinear trend of decreasing strength with increasing moisture content is visible and similar in all the three clays. The findings disagree with the behaviour seen in the comparison between the results of the direct tensile tests found in lab tests and in literature (Figure 13). In the graph, the literature data were overlapping for moisture contents higher than 1.2 meaning that the plasticity index does not have a particular effect on the tensile behaviour of clays. Differently, the results found for Kaolin, Durham and London clay shows a relationship between the tensile strength and the plasticity index and the data are not overlapping on a single curve. However, two different moisture content normalisations were used to plot the data, as two different methods were used to prepare the samples.

Moisture content also affected the ability of the clays to deform (Figures 11 and 12). An increase of moisture content generally determined larger deformations. This behaviour was most markedly observed in kaolin samples, while Durham clay samples did not show variations in deformation during bending tests. London clays had a different behaviour during bending tests because the deformation diminished with the increase of moisture content. Thus, the London clay deformed less than the moderate plasticity kaolin clay. This pattern of strain behaviour could be seen during both the tensile and bending tests.

FRACTURE ANALYSIS IN WET BENDING BEAMS OF MODERATE/HIGH PLASTICITY

Durham clay has a low plasticity index and therefore behaved in an almost elastic manner for the moisture contents ω=17.0-26.6% (ω/LL=0.41-0.64, Fig. 8) analysed. According to the linear elastic fracture mechanics (Janssen, 2002) the plastic zone around the notch tip is so small that it can be considered to not affect the material behaviour. The crack developed instantaneously through the beam thickness leading to an essentially instantaneous failure. Due to the low plasticity of the Durham clay, specimens behaved elastically with an instantaneous crack appearance and failure. For that, the fracture behaviour of the Durham clay was not studied.

As the graphs in Figures 8 and 12 show, plastic clays sustained different amounts of bending deformation before collapsing, with the nonlinear response of London and kaolin clays exhibiting larger deformations compared to the equivalent Durham clay. But London clay deformed less than the kaolin beams, despite the plasticity index of the London clay being higher than that of kaolin clay. Additionally, the crack propagation in London clay was faster than in kaolin clay. The crack propagation in kaolin samples was slower and often in finite increments rather than a smooth progression. This allowed the kaolin samples to sustain more strain before collapse. The difference in crack propagation is seen in Figure 15, where the crack extension is plotted against the vertical displacement of the beams' middle section. The data plotted in the figure were found from the tests on beams with the highest moisture content ratio (ω/LL=0.67 for kaolin and ω/LL=0.66 for London clay). The crack propagation of other two beams of kaolin and London clays are also plotted in the graph. For ω/LL=0.67, kaolin beams reached a displacement of 2 mm before crack initiation. Then, a slow crack growth through finite increments was visible. In the London clay beam (ω/LL=0.40) , the crack was not visible until a displacement of 0.4 mm was reached. It then grew quickly in length. The wettest sample of London clay had the same behaviour, but the crack initiated at higher applied vertical displacement.

The tensile crack developed in two different manners in kaolin and London clays due to the different effects of strain hardening. In kaolin beams, the low yield stress allowed plastic deformation to occur at the tip of the notch until the ultimate tensile strength was exceeded (Figure 16). This response demonstrates that the clay beam could not crack while it was undergoing plastic flow with a stress lower than the ultimate tensile strength. Once the tensile strength was reached, a crack initiated and started to grow in the area where plastic deformation occurred. The crack growth was slow as only a small elastic energy was accumulated before reaching the yield stress. As the test proceeded, the load increased so that a larger volume of clay underwent plastic deformation caused by an applied stress greater than the ultimate tensile strength. This caused further crack growth until the beam was unable to sustain the applied load.

The opposite behaviour was seen in the more plastic London clay (Figure 17). A high yield stress and a small amount of plastic flow resulted in a different crack growth response. Due to the high yield stress, only a small volume of soil around the notch tip underwent plastic deformation. When the ultimate tensile strength was exceeded at the notch tip, the crack developed almost instantaneously as the clay surrounding the notch tip was still in an elastic condition and a high elastic energy was accumulated before reaching the yielding stress.

The strain difference between the clays was predominantly observed at the end of the bending tests, when assessing the sample notch. In kaolin beams the notch passed from a sharp shape to a less defined (blunted) shape in which the notch mouth faces separated and rotated from each other. Once the blunted notch reached a limit value of deformation, a crack developed from one of the notch corners and grew into the beam thickness. London clay samples demonstrated a much sharper fracture with less blunting at the notch tip. This difference is illustrated in Figure 18.

FRACTURE TOUGHNESS IN WET BENDING BEAMS OF MODERATE/HIGH PLASTICITY

The difference in bending behaviour between kaolin and London clays can be studied using the EPFM to determine the fracture toughness of the two clays. In fracture mechanics, the J-integral represents the energy necessary to create a unit area of new crack surface (or energy release rate) in the nonlinear case. Using the energy approach formulated by Rice (1968), the J-integral can be calculated as a path-independent line integral equal to the reduction of potential energy per increment of crack extension. This means that J can be seen as a measure of the intensity of stress and strain at the tip of the notch and crack (Janssen et al. 2002). Thus, the critical value is indicated as J_{IC} and represents the fracture toughness that would be considered in LEFM analysis. The fracture toughness J_{IC} gives an indication of the expected ductility during loading.

For soils there is not a specific method for the determination of the J-integral, so the procedure in ASTM E1820-15 (2015) was used. The standard calculates the J-integral as a sum of an elastic and a plastic component. The elastic component includes the fracture toughness for the linear elastic case, while the plastic component depends on the area under the force-displacement graph and the beam's thickness. Once the J-integral is calculated at different stages of the test, the critical value is determined. Figure 19 summarises the procedure used to calculate J_{IC}. Some corrections to the method were made to calculate the M parameter necessary to use the equation $J = M\sigma_Y \Delta a_{max}$. For metals the M parameter is constant and fixed with M=2. In the soil case, the M parameter was calculated using a similar equation which links the yield stress to the crack tip opening angle via $J = M\sigma_{YS}\delta_t$ and M was determined experimentally as the gradient of the linear approximation curve that fitted the J - δ_t data, where δ_t is the crack width at the base of the notch. Differently from metals, the M parameter varied with the variation of the moisture content. In Figure 20 the variation of the M parameter in relation to the normalised moisture content is plotted. The data shown in the figure are related to the kaolin samples studied in the fracture analysis.

The fracture toughness determined for kaolin and London clays is shown in Figure 21, where it has been related to the moisture content. The fracture analysis was performed using digital images to track the development of the crack on the beam surface. The fracture analysis on Durham clay beams was not possible due to the instantaneous crack propagation and the inability to track the development of the crack tip. However, the range of moisture content used to test the Durham clay bending samples was reported in Figure 21on the x-axis while on the y-axis the corresponding J_{IC} was considered null, because it was not calculated.

Looking at Figure 21 London clay samples had lower values of fracture toughness than kaolin. The results validate the strain hardening behaviour shown in Figure 17, as the low fracture toughness indicates a fragile failure for crack propagation. In addition, the data plotted on the graph shows that the fracture toughness found in London clay dropped steeply when the moisture content increased toward the limit liquid. On the other side, kaolin beams had high values of fracture toughness which were higher than those of London clay. The fracture toughness of kaolin proved that kaolin failed in a more ductile manner during the experiments. A difference in behaviour between the samples of kaolin and London clay is explained considering the formula used to calculate J_{IC} (Janssen 2002):

$$J_{IC} = \frac{\eta U_{cr}}{Bb} \qquad (10)$$

in which η is an empirical constant usually equal to 2, U_{cr} is the area under the load-displacement curve at the onset of the crack extension, B is the sample width and b=W-a is the resistant ligament length. For kaolin samples, the area under the load-displacement curve had a high value thanks to the large displacements developed and remained almost constant with various moisture contents. In London clay, the area under the load-displacement curve varied due to the fact that drier samples sustained more deformation than wetter samples and therefore J_{IC} decreased steeply at high moisture contents.

Similarly to the tensile behaviour, the values of fracture toughness calculated for kaolin and London clays did not fall on the same line. In the case of PI=31% (kaolin) and PI=41.8% (London clay), the plasticity index is influencing the fracture toughness. The J-integral results diminished with the increase of moisture content, similarly to what was seen for the tensile and flexural strength. Values of the J-integral plotted in Figure 21 shows both the dependence of the clays to the plasticity index and the moisture content.

6. CONCLUSIONS AND FUTURE WORK SUGGESTIONS

Overall, the paper has shown that the Elasto-Plastic Fracture Mechanic theory can be applied to clay soils in situations prone to tensile failures (e.g. sinkhole formation), and that there is a clear link between moisture content and fracture toughness of clay soils. Given the range of conditions tested, the following conclusions can be made:

- Tensile behaviour of clay is controlled by the moisture content, showing a non-linear reduction in strength with increasing moisture content. Maximum values of strength are recorded for normalised moisture content of 0.30-0.40.
- Plasticity index appears to affect tensile and fracturing behaviour of clays. This is visible in particular analysing the fracturing process, where a more plastic clay developed a fragile collapse for fracture propagation. A moderate plasticity clay showed a ductile behaviour and failure for crack propagation.

Further work is necessary to refine the application of the ASTM E1820-15 (2015) standard method for assessing fracture toughness when applied to soils. In the studied cases, the fracture toughness determined by applying the ASTM E1820-15 (2015) standard validates the behaviour seen during the tests, even if some coefficients were not modified from the metallic to the soil application.

This investigation highlighted the importance of studying fine-grained soils under tensile loads. This area is especially critical for the study of sinkhole formation, in particular for the study of the soil covering underground cavities. Despite the results are not directly applicable to sinkhole events, the results show that moisture content can be used in future to study and even predict sinkholes. For example, following heavy rainfall events, high moisture content clays might be seen as critical and in need of monitoring in areas where the presence of a cavity is known.

Many aspects of this investigation can be developed for a better understanding of cracked clays. Different geometries can be considered in the experiments for a better simplification of the sinkhole geometry. Deep beams, thin plates or bending beams with different heights are suggested to be studied to confirm the failure in finite increments. In addition, suction should be measured during direct tensile and bending tests to understand how it affects the cracking process. Refinements to the method used for testing clays and analysing the data are also suggested. For example, the GeoPIV technique is proposed to determine the stress development on the surface of the samples during the tests, as done by Thusyanthan et al., 2007. From the tests performed on kaolin and London clays modifications to the test geometry reported in the ASTM E1820-15 (2015) standard are suggested to consider the soft nature of a clay. Then, the ASTM E1820-15 (2015) method is using various empirical coefficients that are calibrated on the tests results on metals and need to be validated for the soil case. The calculations for the J-integral and the assumptions for the value of the M-coefficient may need to be refined based on information from more clay types and conditions.

7. ACKNOWLEDGMENTS

The paper is based on the research done during my PhD (Forlati, 2016) which was gratefully supported by the Engineering and Physical Sciences Research Council (Grant No. 1524864).

8. REFERENCES

Abdulla, W. A. and Goodings, D. J. (1996). Modelling of sinkholes in weakly cemented sand. Journal of Geotechnical Engineering 122(**12**)

Ajaz, A. and Parry, R. H. G. (1975). Stress-strain behaviour of two compacted clays in tension and compression. Géotechnique **25**(3), 495-512.

Amarasiri, A. L., Costa, S. and Kodikara, J. (2011). Determination of cohesive properties for mode I fracture from compacted clay beams. Canadian Geotechnical Journal **38**, 1163-1173.

Anderson, T. L. (2005). Fracture Mechanics. Fundamentals and applications. Taylor& Francis.

ASTM E8/E8M-15a (2015). Standard test method for tension testing of metallic materials.

ASTM E1820-15 (2015). Standard test method for measurement of fracture toughness.

Bronkhorst, W. P. and Jacobsz, S. W. (2014). The behaviour of weakly cemented sand beams spanning over openings, *In* Physical Modelling in Geotechnics, Gaudin & White (Eds), pp 1107-1112

BS 1377-4:1990. Methods of tests for soils for civil engineering purposes. Compaction-related tests.

Donnelly, L. J. (2008), `Subsidence and associated ground movements on the Pennines, northern England', Quarterly Journal of Engineering Geology and Hydrogeology **41**, 315-332.

Forlati G. (2016). Fracture behaviour of clayey soils overlying cavities. PhD Thesis, Department of Civil and Structural Engineering, The University of Sheffield, Sheffield, UK.

Gasparre, A. (2005). Advanced laboratory characterisation of London clay. PhD Thesis, Department of Civil and Environmental Engineering, Imperial College, London, UK.

Glendinning, S., Hughes, P., Helm, P., Chambers, J., Mendes, J., Gunn, D., Wilkinson, P. and Uhlemann, S. (2014). Construction, management and maintenance of embankments used for road and rail infrastructure: implications of weather induced pore water pressures. Acta Geotechnica **9**, 799-816.

Hallett, P. D. and Newson, T. A. (2001). A simple fracture mechanics approach for assessing ductile crack growth in soil. Soil Science Society of America Journa l**65**, 1083-1088.

Hallett, P. D. and Newson, T. A. (2005). Describing soil crack formation using elastic-plastic fracture mechanics. European Journal of Soil Science **56**, 31-38.

Janssen, M., Zuidema, J. and Wanhill, R. J. H. (2002). Fracture Mechanics. SponPress.

Lakshmikantha, M. R., Prat, P. C., Tapia, J. and Ledesma, A. (2008). Effect of moisture content on tensile strength and fracture toughness of a silty soil, *In* C. Press, ed., Proceedings of the first European Conference on Unsaturated soils, pp. 405-409.

Mavroulidou, M., Zhang, X., Kichou, Z. and Gunn, M. (2013). Hydro-mechanical properties of lime-treated London clay, *In* Proceedings of the 18th International Conference on Soil Mechanics and Geotechnical Engineering, pp. 1151-1154.

Murillo, C., Caicedo, B., Thorel, L., Dano, C. (2013). Elastic response of unsaturated soils, *In* Unsaturated Soils, Taylor & Francis Group, London, pp. 321-327.

Rice, J. R. (1968). A path independent integral and the approximate analysis of strain concentration by notches and cracks. Journal of Applied Mechanics **35**, 379-386.

Sinkholes | British Geological Survey http://www.bgs.ac.uk/research/engineeringGeology/shallowGeohazardsAndRisks/sinkholes/home.html [access January 2014]

Sivakumar, V., Anderson, C., Solan, B., Rankin, B. and Mackinnon, P. (2015). Influence of testing on permeability of compacted fine soils, *In* ICE Proceedings. Geotechnical Engineering, Vol. 168, pp. 422-438.

Stirling, R. A., Hughes, P., Davie, C. T. and Glendinning, S. (2015). Tensile behaviour of unsaturated compacted clay soil - A direct assessment method, Applied Clay Science **112-113**, 123-133.

Tang, C., Pei, X., Wang, D., Shi, B. and Li, J. (2015). Tensile strength of compacted clayey soil. Journal of Geotechnical and Geoenvironmental Engineering **141** (4),65-75.

Thusyanthan, N., W. A. Take, Madabhushi, S. P. G., Bolton B. D. (2007). Crack initiation in clay observed in beam bending. Geotéchnique **57,** 581-594.

Toll, D. G., Mendes, J., Gallipoli, D., Glendinning, S., Hughes, P. N. (2012). Investigating the impacts of climate changes on slopes. Geological Society, London, Engineering Geology Special Publications **26**, 151-161.

Tschebotarioff, G. P., Ward, E. R. and DePhilippe, A. A. (1953). The tensile strength of disturbed and recompacted soils, *In* `Proceedings of the 3rd International Conference on Soil Mechanics and Foundation Engineering, Vol. 1, pp. 207-210.

Viswanadham, B. V. S., Jha, B. K. and Pawar, S. N. (2010). Experimental study on flexural testing of compacted soil beams. Journal of Materials in Civil Engineering **22**, 460-468.

Waltham, T., Bell, F. and Culshaw, M. (2005). Sinkholes and subsidence. Karst and cavernous rocks in engineering construction. Praxis Publishing, Chichester, UK.

Wang, J., Zhu, J., Chiu, C. F. and Zhang, H. (2007a). Experimental study on fracture behaviour of a silty clay. Geotechnical Testing Journal **30**(4), 309-322.

TABLES

Soil name	LL (%)	PL (%)	PI (%)	Activity	ω_{OMC} (%)
Speswhite kaolin	65.0	34.0	31.0	0.39	34.0
Durham clay	41.7	23.3	18.4	0.50	15.5[a]
London clay	75.3	33.5	41.8	0.58-0.99	24.5[b]

Table 1: Geotechnical properties of the three study clays

[a]Glendinning et al. (2014)

[b]Sivakumar et al. (2015), Mavroulidou et al. (2013)

FIGURE CAPTIONS

Figure 1: Process of sinkhole formation in a clay layer

Figure 2: Mechanical model used to simplify the mechanism of sinkhole formation

Figure 3: Typical particle size distribution found for kaolin, Durham and London clays.

[a] Particle size distribution taken from Murillo et al. (2013)

[b] Particle size distribution taken from Toll et al. (2012)

[c] The two dashed lines represent the upper and lower limits of the passing percentages

[d] Particle size distribution taken from Gasparre (2005)

Figure 4: Tensile (a) and bending (b) samples used for direct tensile and bending tests

Figure 5: Samples shape for the direct tensile test (a) and for the bending test (b)

Figure 6: Net section in bending beams

Figure 7: Example of stress-strain graph obtained from direct tensile tests

Figure 8: Example of stress-strain graph obtained from bending tests

Figure 9: Tensile strength calculated from direct tensile tests

Figure 10: Flexural strength determined from bending tests

Figure 11: Strain recorded at the maximum tensile stress in direct tensile tests

Figure 12: Strain recorded at the maximum flexural stress in bending tests

Figure 13: Tensile strength comparison between the tested clays and literature results. [a] load-controlled tests, [b] strain-controlled tests.

Figure 14: Tensile strengths calculated from direct tensile and bending tests

Figure 15: Crack growth progression

Figure 16: Strain hardening and crack propagation in a kaolin clay sample

Figure 17: Strain hardening and crack propagation in a London clay sample

Figure 18: Initial notch deformation in London (a) and kaolin (b) samples having respectively $\omega/LL = 0.41$ and $\omega/LL = 0.66$

Figure 19: ASTM E1820-15 (2015) process to determine J_{IC}

Figure 20: Variation of the M parameter with the moisture content in kaolin samples

Figure 21: Variation of fracture toughness J with moisture content

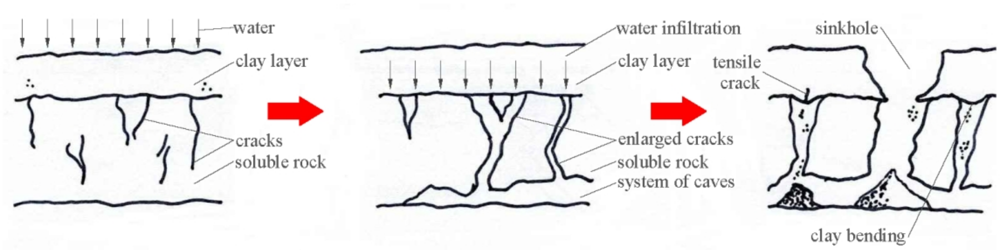

Figure 1: Process of sinkhole formation in a clay layer

209x148mm (193 x 193 DPI)

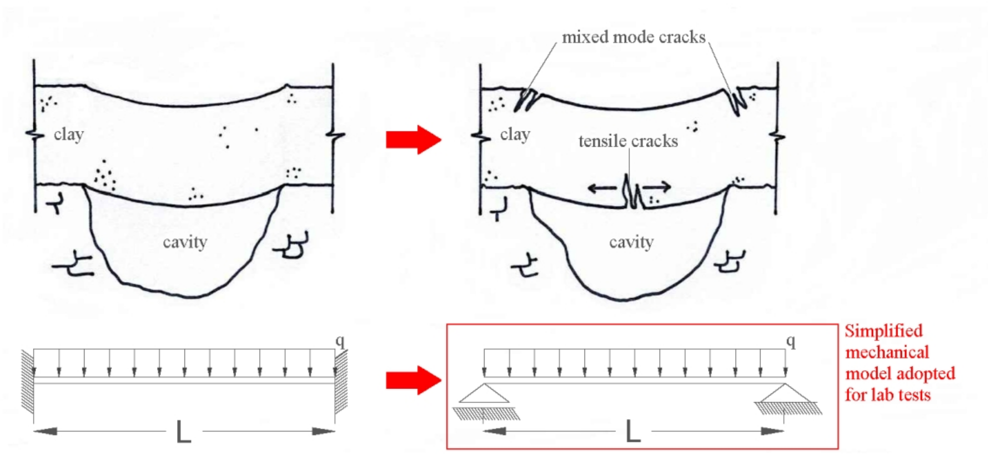

Figure 2: Mechanical model used to simplify the mechanism of sinkhole formation

209x148mm (193 x 193 DPI)

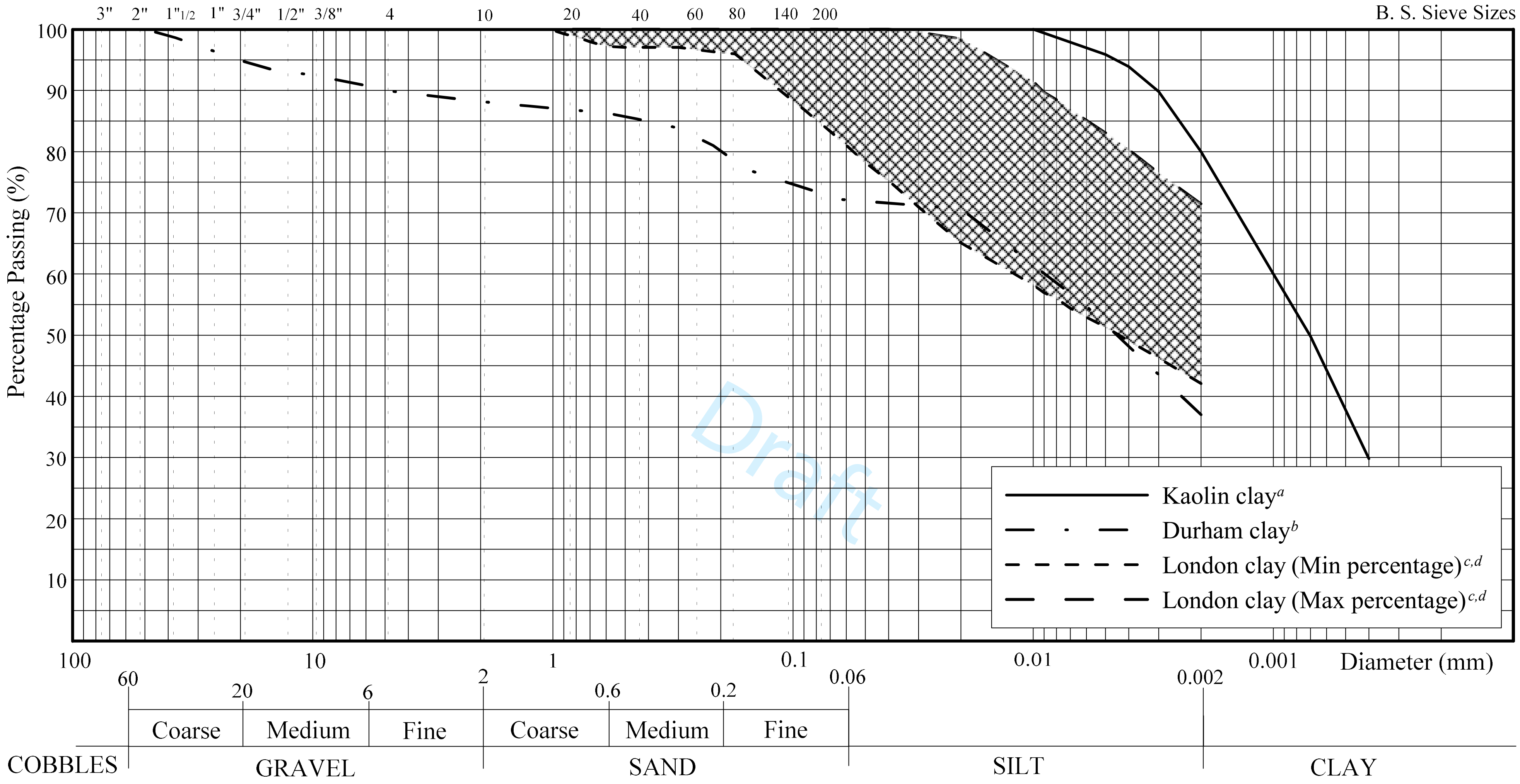

Figure 3: Typical particle size distribution found for kaolin, Durham and London clays.

[a]Particle size distribution taken from Murillo et al. (2013)

[b]Particle size distribution taken from Toll et al. (2012)

[c]The two dashed lines represent the upper and lower limits of the passing percentages

[d]Particle size distribution taken from Gasparre (2005)

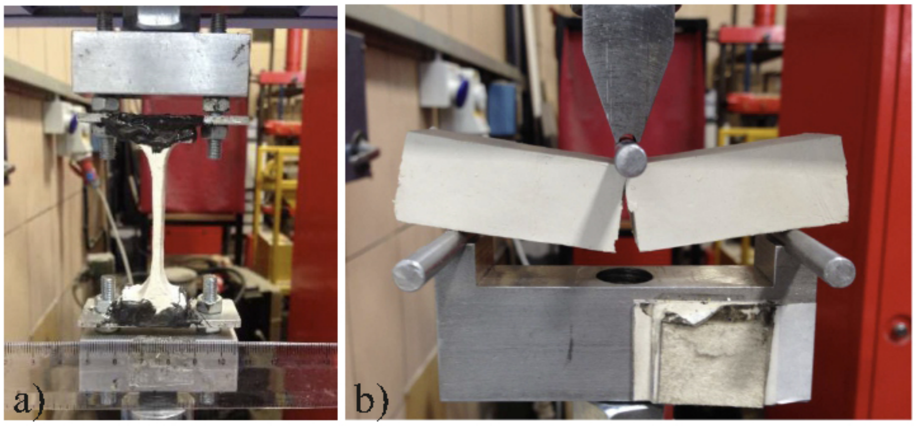

Figure 4: Tensile (a) and bending (b) samples used for direct tensile and bending tests

100x50mm (200 x 200 DPI)

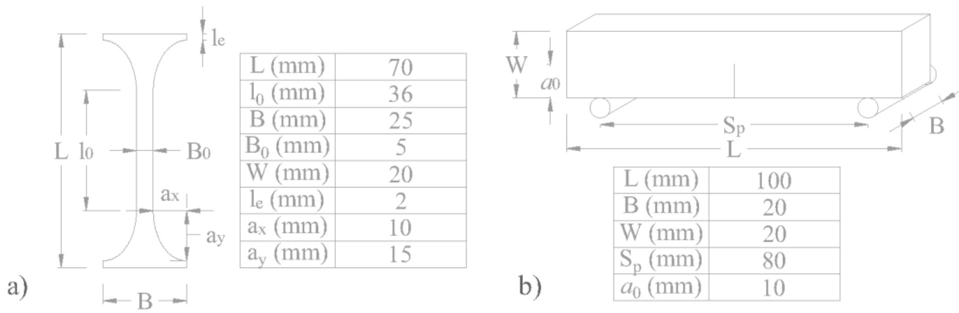

Figure 5: Samples shape for the direct tensile test (a) and for the bending test (b)

199x69mm (200 x 200 DPI)

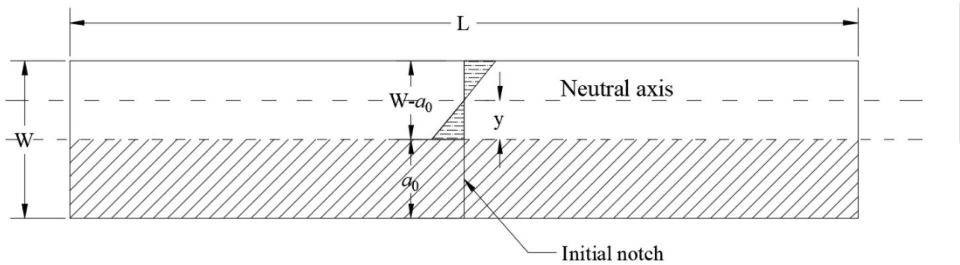

Figure 6: Net section in bending beams

279x215mm (135 x 135 DPI)

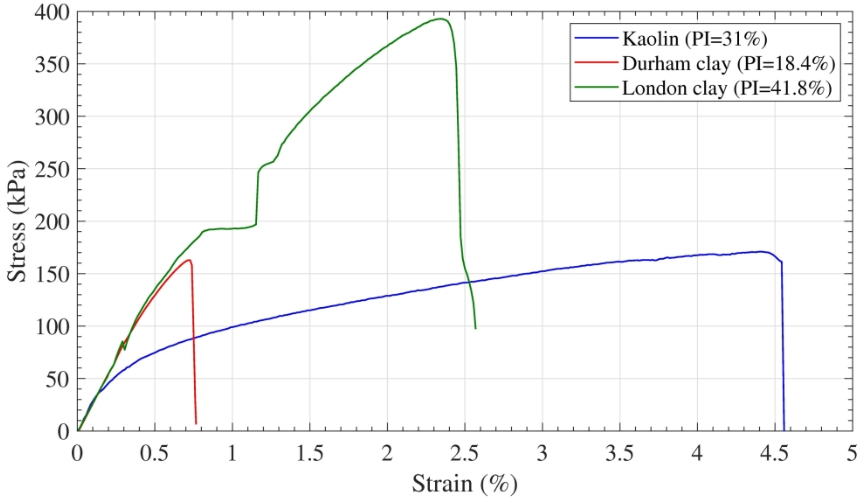

Figure 7: Example of stress-strain graph obtained from direct tensile tests

240x126mm (300 x 300 DPI)

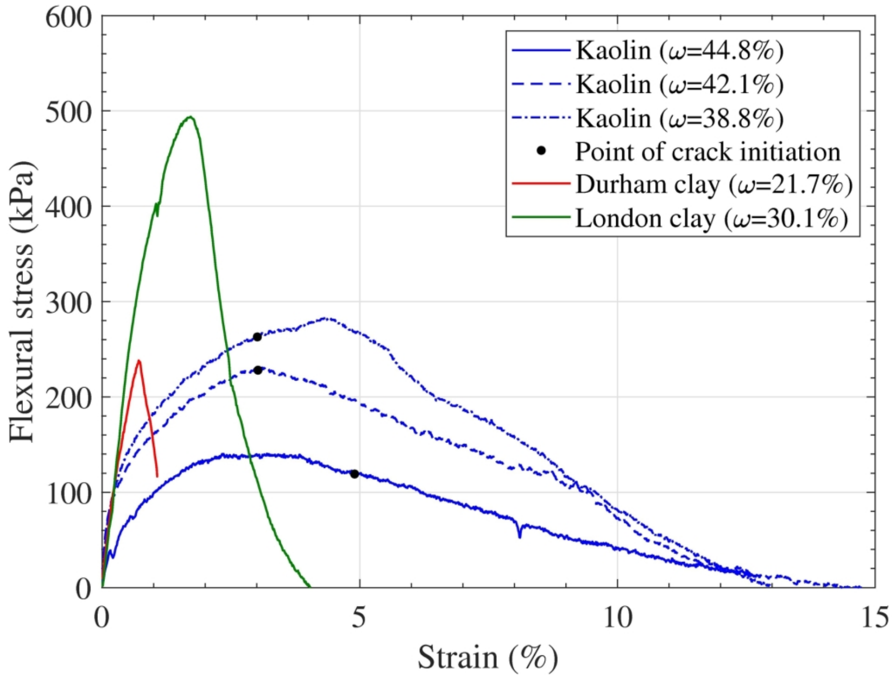

Figure 8: Example of stress-strain graph obtained from bending tests

180x128mm (300 x 300 DPI)

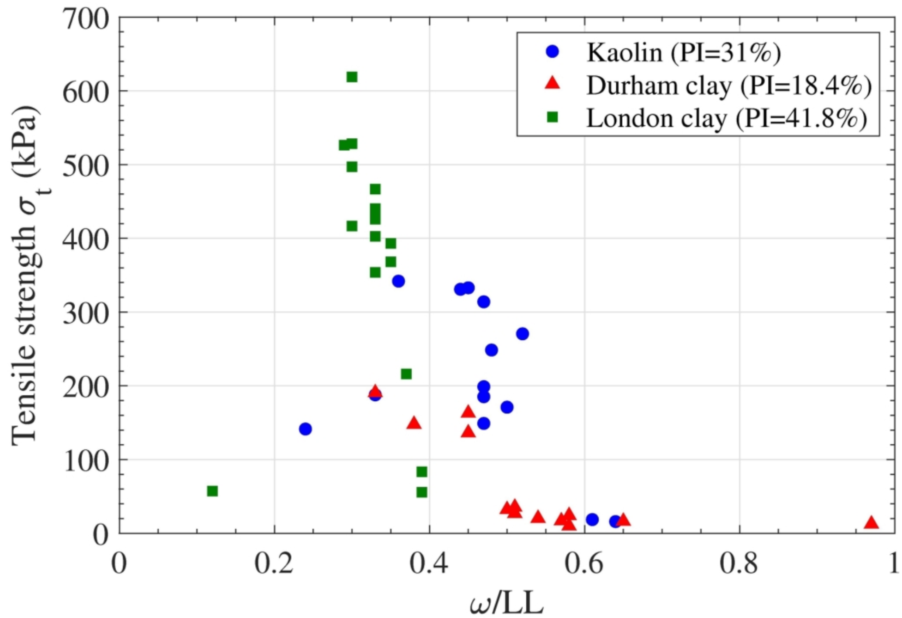

Figure 9: Tensile strength calculated from direct tensile tests

179x117mm (300 x 300 DPI)

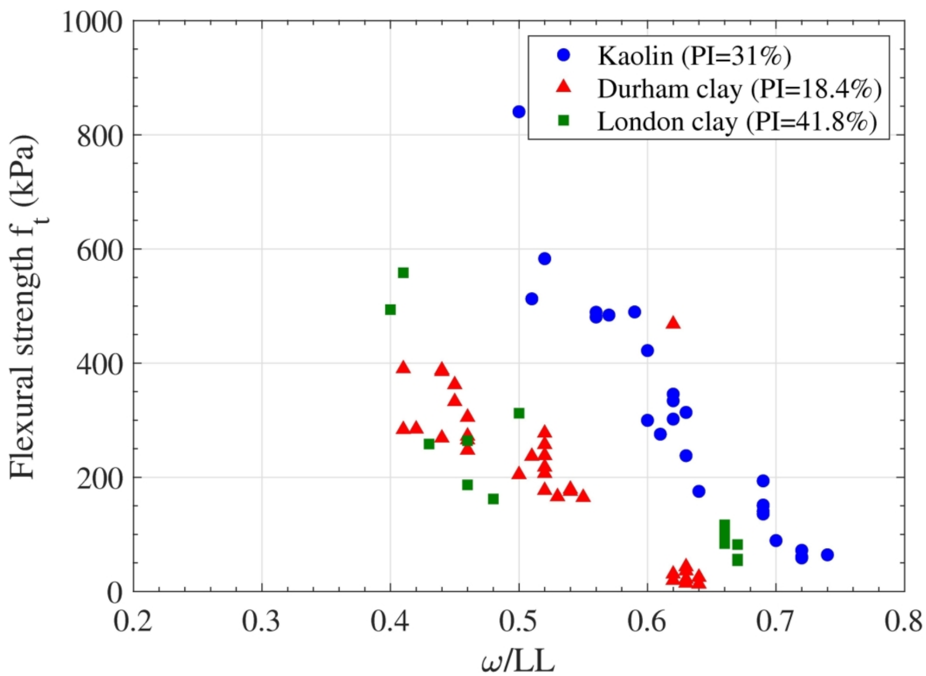

Figure 10: Flexural strength determined from bending tests

180x128mm (300 x 300 DPI)

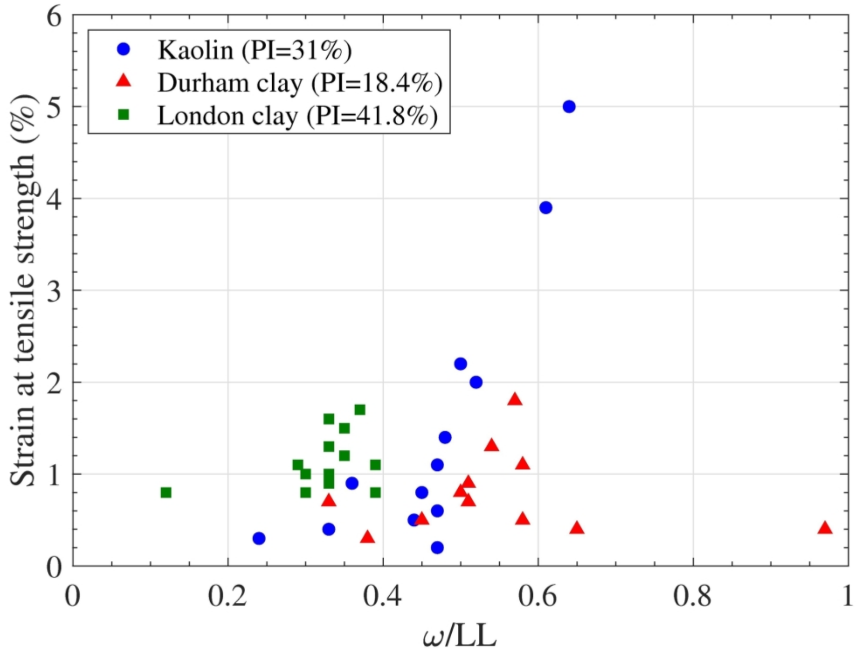

Figure 11: Strain recorded at the maximum tensile stress in direct tensile tests

180x124mm (300 x 300 DPI)

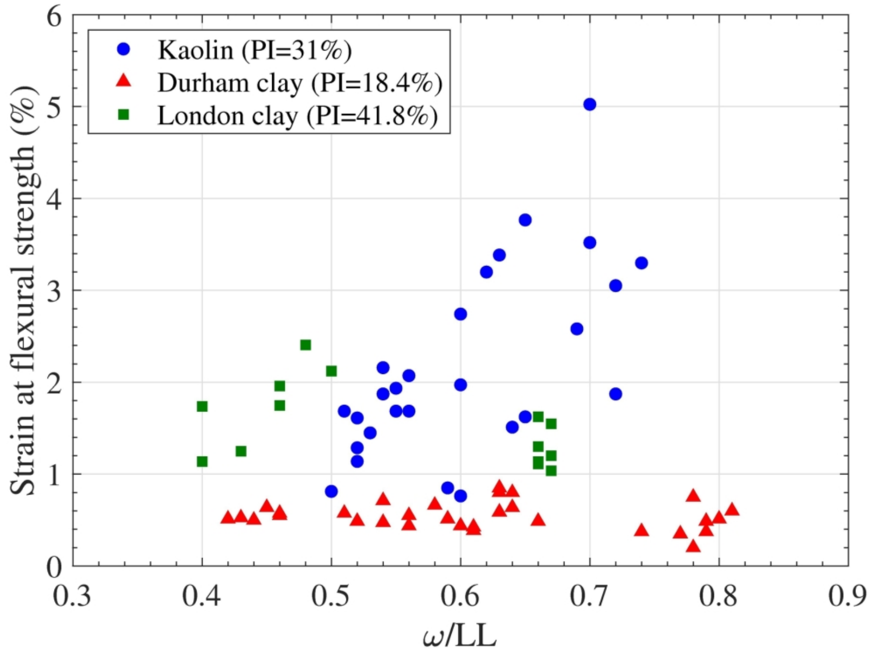

Figure 12: Strain recorded at the maximum flexural stress in bending tests

180x124mm (300 x 300 DPI)

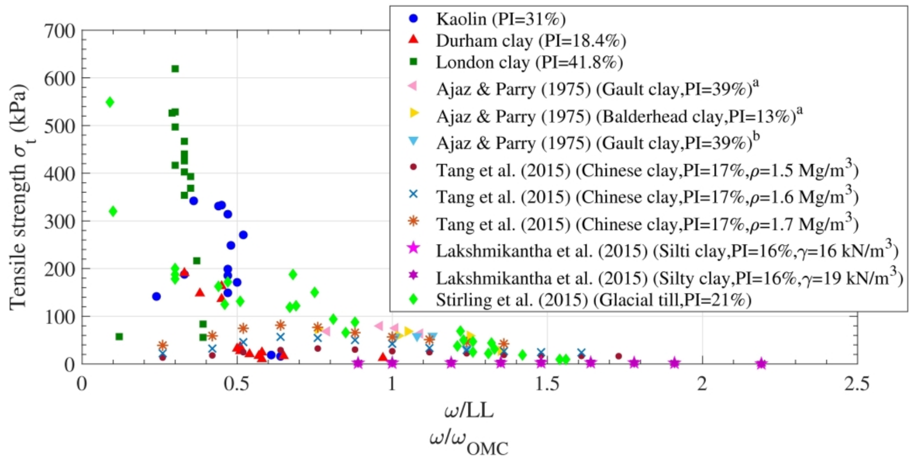

Figure 13: Tensile strength comparison between the tested clays and literature results. a load-controlled tests, b strain-controlled tests.

270x125mm (300 x 300 DPI)

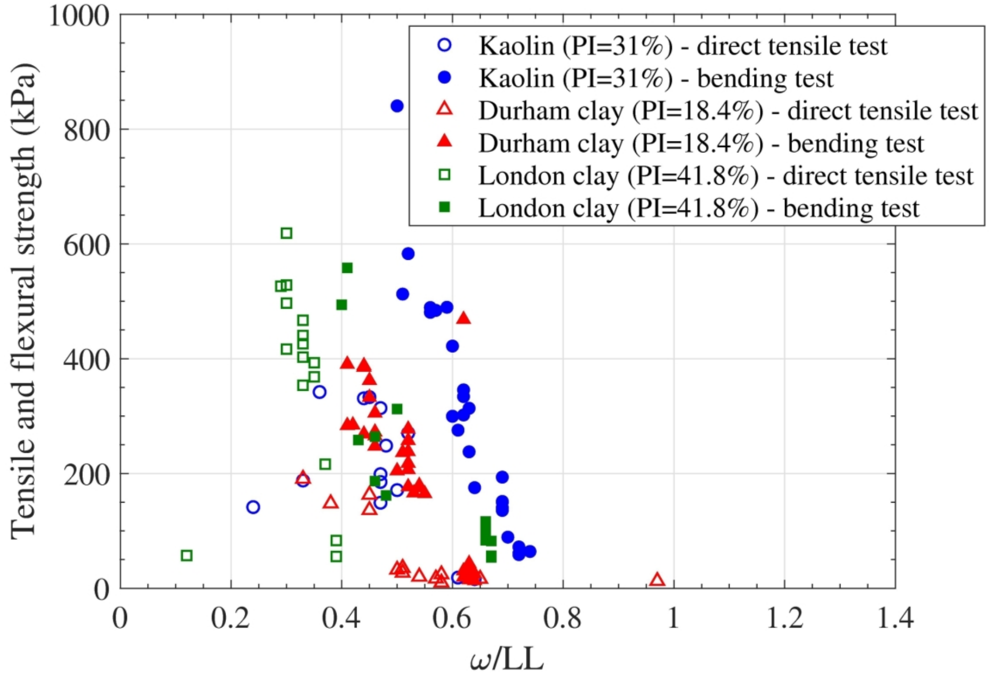

Figure 14: Tensile strengths calculated from direct tensile and bending tests

180x129mm (300 x 300 DPI)

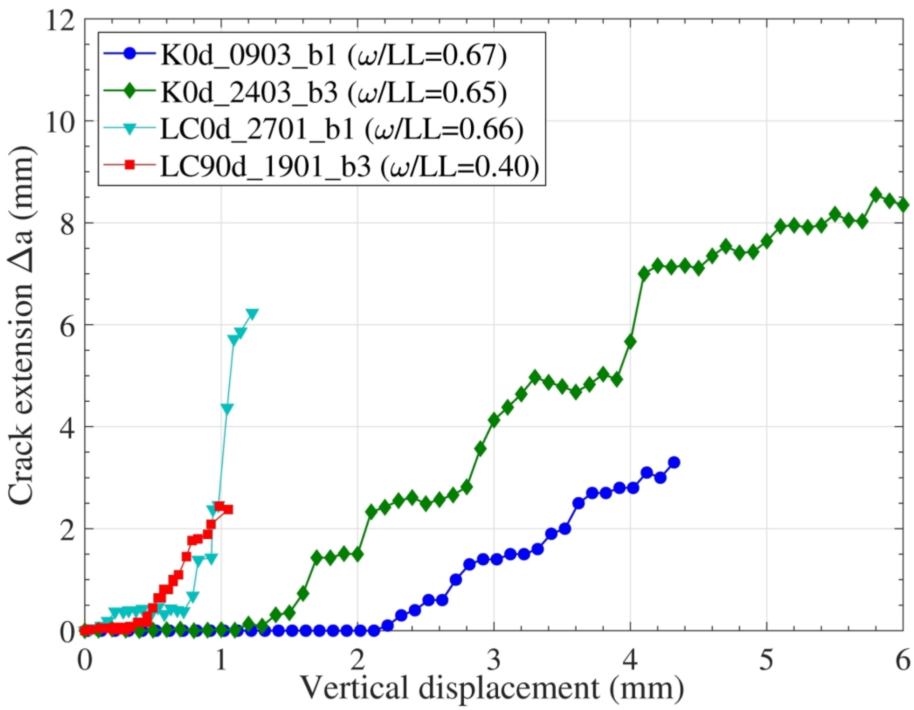

Figure 15: Crack growth progression

203x152mm (300 x 300 DPI)

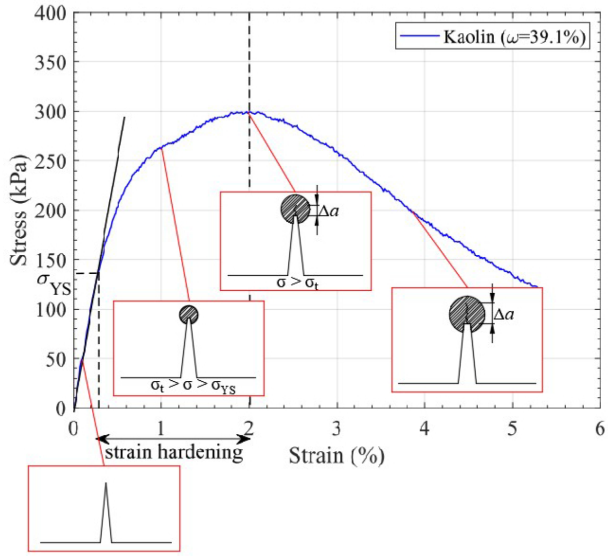

Figure 16: Strain hardening and crack propagation in a kaolin clay sample

279x215mm (96 x 96 DPI)

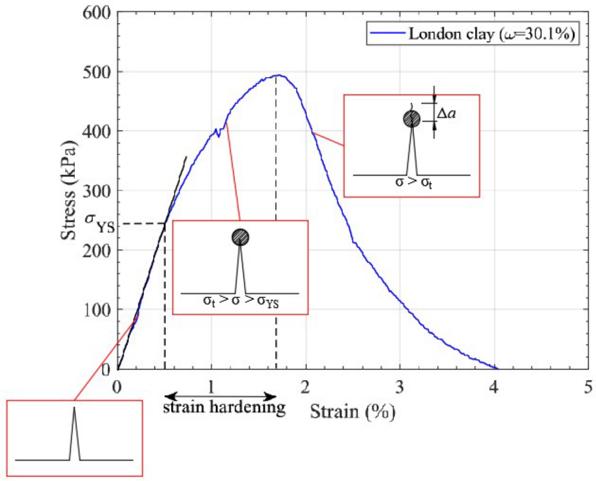

Figure 17: Strain hardening and crack propagation in a London clay sample

279x215mm (96 x 96 DPI)

Figure 18: Initial notch deformation in London (a) and kaolin (b) samples having respectively ω/LL=0.41 and ω/LL=0.66

120x50mm (120 x 128 DPI)

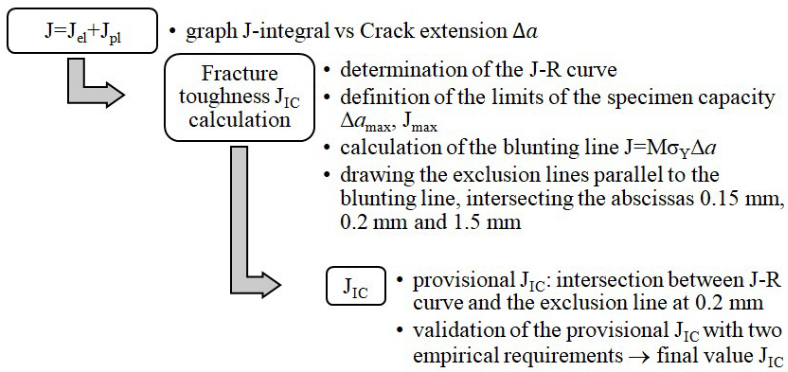

Figure 19: ASTM E1820-15 (2015) process to determine JIC

279x215mm (96 x 96 DPI)

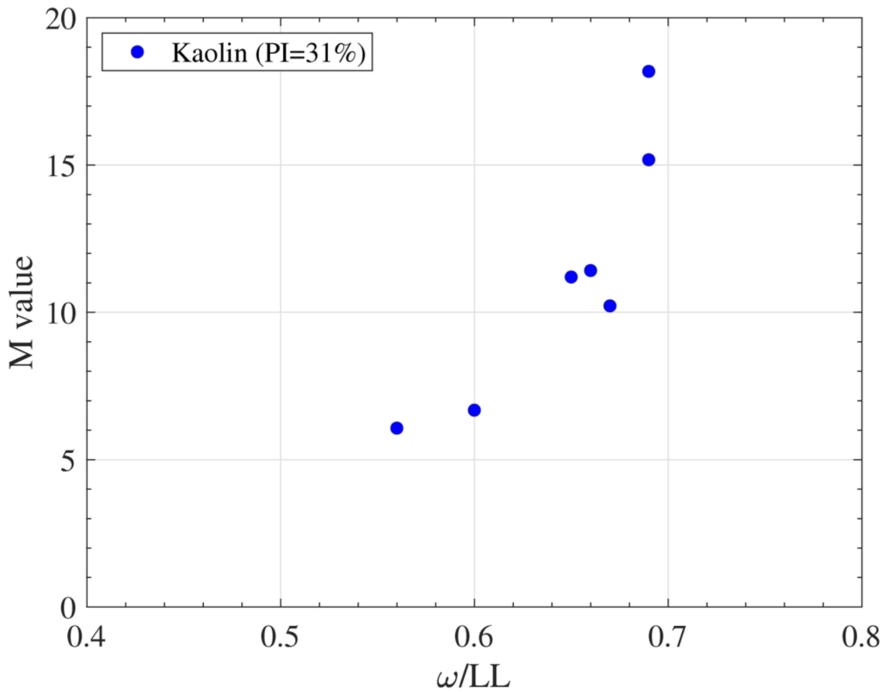

Figure 20: Variation of the M parameter with the moisture content in kaolin samples

180x131mm (300 x 300 DPI)

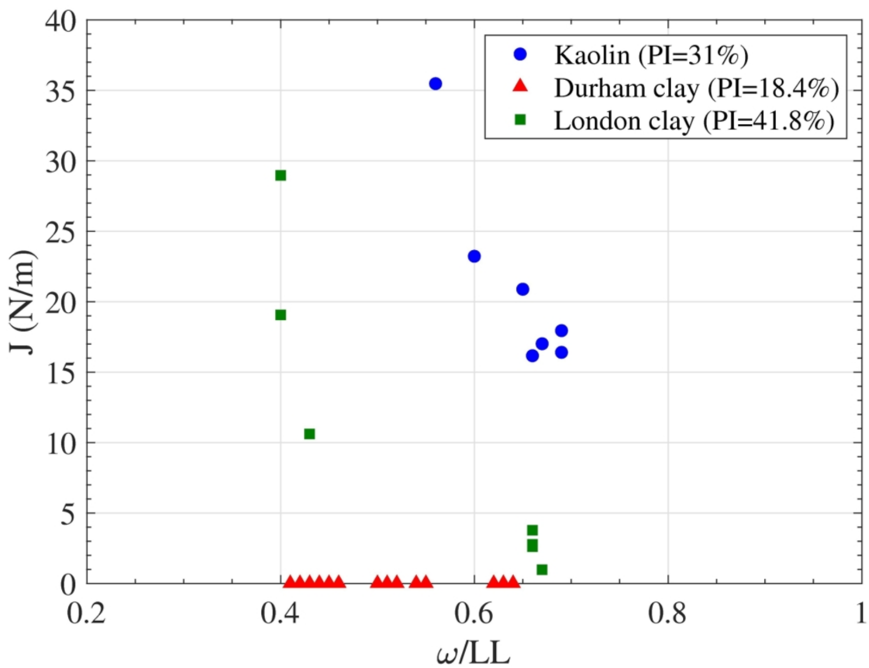

Figure 21: Variation of fracture toughness J with moisture content

180x127mm (300 x 300 DPI)